JOURNAL OF THERMAL STRESSES
https://doi.org/10.1080/01495739.2023.2193225

Taylor & Francis
Taylor & Francis Group

Simulation of wave propagation in thermoporoelastic media with dual-phase-lag heat conduction

Yunfei Liu[a,b], Li-Yun Fu[a,c], Wubing Deng[a,c], Wanting Hou[a,b], José M. Carcione[d], and Jia Wei[e]

[a]Shandong Provincial Key Laboratory of Deep Oil and Gas, China University of Petroleum (East China), Qingdao, China; [b]School of Geosciences, China University of Petroleum (East China), Qingdao, China; [c]Laboratory for Marine Mineral Resources, Qingdao National Laboratory for Marine Science and Technology, Qingdao, China; [d]National Institute of Oceanography and Applied Geophysics – OGS, Trieste, Italy; [e]Institute of Geology and Geophysics, Chinese Academy of Sciences, Beijing, China

ABSTRACT

The theory of wave propagation in non-isothermal porous rocks has been introduced in geophysics in recent years by combining the single-phase-lag (SPL) Lord-Shulman (LS) model of heat conduction with Biot's poroelasticity theory. However, the theory of SPL thermoporoelasticity is inadequate in describing the lagging behavior of thermal relaxation for wave dissipation due to fluid and heat flow effects. We address this problem by incorporating a dual-phase-lags (DPL) model of heat conduction into thermoporoelasticity, utilizing analytical solutions and numerical simulations. The DPL model involves two lagging times: the (macroscopic) heat-flux lagging time τ_q from the LS model and an additionally introduced lagging time τ_T of temperature gradient that characterizes the fluid phase. A plane-wave analysis predicts four propagation waves, namely, fast P, slow P, thermal (T), and shear (S). We calculate wavefield snapshots by using a finite-difference solver for the DPL thermoelastic equations and provide further insight into the physics of two lagging times for porous rocks. The simulations show that the DPL model induces higher thermal attenuation and larger velocity dispersion compared to the SPL model, especially at high frequencies. The influence of fluids is crucial for wave propagation within thermoporoelastic media.

ARTICLE HISTORY
Received 12 August 2022
Accepted 6 March 2023

KEYWORDS
Double-phase-lag model; microscopic effects; thermal relaxation; thermoporoelasticity; wave propagation

1. Introduction

The study of wave propagation in non-isothermal media is significant in various fields, including earthquake seismology, geothermal exploration, thermal-enhanced oil recovery, and ultradeep hydrocarbon exploration (e.g., [1–3]).

The previous theory of thermoelasticity [4–6], which is based on the parabolic equation of heat conduction, describes the coupling between the fields of displacement and temperature but predicts infinite velocities for thermal waves. This problem has been solved by introducing a delay term into the heat equation [1, 2, 7–10]. In particular, Carcione et al. [2] solved the new thermoelastic equations with the Fourier pseudospectral method to compute the spatial derivatives, and Wang et al. [11] derived the second-order tensor Green's function based on the Lord-Shulman (LS) equations. The LS theory predicts three propagation modes, namely, a fast P wave

CONTACT Li-Yun Fu lfu@upc.edu.cn Shandong Provincial Key Laboratory of Deep Oil and Gas, China University of Petroleum (East China), Qingdao 266580, China.

(E wave), a slow thermal P wave (T wave), and a shear wave (S wave). The P and T modes are dispersive and lossy, presenting similar characteristics of the fast and slow P waves in poroelastic media. Hou et al. [12] investigated the effect of thermal properties (thermal conductivity, thermal expansion coefficient, and specific heat) on wave velocity and attenuation. Much attention has been paid to analytical solutions of wave-induced thermoelastic attenuation and associated thermoviscoelasticity mechanisms based on the Kelvin-Voigt model [13–16], including the more general Zener and Cole-Cole models [17–19]. A detailed discussion on the effect of the lagging time on the attenuation peak and relaxation frequency is referred to Carcione et al. [2].

Thermoporoelasticity combines Biot's equations and classical heat conduction [20, 21]. The dynamical equations predict four propagation modes (e.g., [9]), namely, those mentioned above and the slow (Biot) P diffusion/wave. The shear wave is unaffected by the thermal effects in homogeneous media. By using the LS model of heat conduction with a single-phase-lag (SPL) time, Carcione et al. [1] performed wave simulations with the Fourier pseudospectral method and showed that the thermal and Biot slow wave have the same behavior, that is, diffusive at low frequencies and wave-like at high frequencies. The conversion of P waves to Biot and thermal modes leads to the so-called mesoscopic energy attenuation [17]. Wei et al. [22] formulated a frequency-domain Green function as a displacement-temperature solution of the SPL thermoporoelasticity equations to investigate the effect of fluid viscosity and thermal properties. Kumar et al. [23] generalized the theory to a double-porosity structure of pores and cracks, but the theory predicts negative dissipation factors, indicating instability. Li et al. [24] incorporated the SPL model into the Biot-Rayleigh double-porosity theory [25] to obtain a double-porosity thermoporoelasticity theory that predicts positive dissipation factors. Wang et al. [26] developed a generalized thermoporoelasticity theory, including the LS and Green-Lindsay models with a SPL for wave propagation in partially saturated media.

The lagging time is closely related to the nonequilibrium features of the thermodynamic transitions. Hetnarski and Ignaczak [27] examined various heat conduction equations used in thermoelasticity. The heat conduction process in the SPL thermoelastic and thermoporoelastic models is described by the Cattaneo-Vernotte (CV) equation [28–30], where the lagging time τ_q of heat flow controls the macroscopic transition from diffusion to wave behavior. An extensive literature has been devoted over the years to heat transfer processes concerning the CV model [31–33]. However, the phase lag of the heat-flux vector tends to induce thermal waves with sharp wavefronts that separate heated and unheated regions because the CV model ignores spatial microscopic effects. Considering the difference between model predictions and experimental results, more targeted and detailed heat conduction models have been proposed. By introducing a lagging time corresponding to the spatial interaction, Qiu and Tien [34] proposed a two-step model from the microscopic phonon-electron perspective to better predict the surface reflectance of metal thin layers. Tzou [35, 36] and Chandrasekharaiah [37] proposed a dual-phase-lag (DPL) model that incorporates microscopic effects into the macroscopic formulation through a lagging time τ_T, which is related to temperature gradients (TGs). The DPL model combines diffusion and wave behavior, and fits well the properties of metallic materials with delay times on the picosecond level [36] and of biological materials on the microsecond or second level [38–42]. For porous rocks, microscopic effects are also particularly important for energy transport and are attributed mainly to the pore-fluid phase, as demonstrated in this study.

We simulate wave propagation in two-phase porous media with dissimilar thermal properties based on the theory of DPL thermoporoelasticity. The heat-flux lagging time τ_q and the TG lagging time τ_T are incorporated into the model. The article is organized as follows. First, we briefly introduce the DPL model and incorporate it into the theory of LS thermoporoelasticity to characterize the microscopic effects. Then, the velocity and attenuation as a function of frequency is obtained by a plane-wave analysis. Next, we model the wavefields by solving the DPL thermoporoelastic equations with the rotated staggered-grid (RSG) finite-difference (FD) method [43–45]

and analyze the physics. Finally, we provide further insight into the physics of the two lagging times for porous rocks by comparing thermal relaxations for wave dissipation based on experimental data from metallic materials and sandstones.

2. DPL thermoporoelasticity theory

Due to the difference in thermal properties between the pore infill (fluid) and frame, it is necessary to consider the microscopic space interaction in the heat transfer process. In comparison to the CV theory used in the SPL model, the DPL theory accurately describes the transmission of thermal energy at very short spatial and/or temporal scales, which avoids the underestimation of thermal effects on wave dissipation. Two distinct lagging times are involved in the transient process. The majority of thermal energy is transmitted into the background medium, where the heat-flux lagging time τ_q represents an average time delay of this process [46]. The TG lagging time τ_T is interpreted by Tzou [46] particularly as "the delay time … caused by the microstructural interactions (small-scale heat transport mechanisms occurring in microscale, or smallscale effects of heat transport in space)."

2.1. Heat conduction

Heat transport occurring at time t can be described by the following energy equation [47],

$$-\nabla \cdot \mathbf{q}(\mathbf{r},t) + S(\mathbf{r},t) = C_p \frac{\partial T_a(\mathbf{r},t)}{\partial t}, \tag{1}$$

where $\mathbf{q}$ is the heat-flux vector, T_a is the absolute temperature, S is the heat source, C_p is the bulk-specific heat of the unit volume at constant pressure, and $\mathbf{r}$ is the space variable. Considering the micro-spatial interaction in rocks, two lagging times are involved in the following constitutive equation,

$$\mathbf{q}(\mathbf{r}, t+\tau_q) = -\gamma \nabla T_a(\mathbf{r}, t+\tau_T), \tag{2}$$

where γ is the bulk coefficient of heat conduction (or thermal conductivity). We refer to the physical and theoretical explanations of heat conduction in metallic phonon-electron and sand bed solid-gas interactions. The lagging times τ_q and τ_T correspond to the delays in the transport of two distinct energy carriers [36, 46], where τ_q is the heat-flux lagging time, which can be regarded as the lag in the overall background heat transfer of the rock, and τ_T is the additional lagging time due to the fluid. Both lagging times are assumed to be intrinsic thermal properties of thermoporoelastic materials, related to the thermal properties of the solid and fluid phases.

Equations (1) and (2) describe the delay behavior in heat transport by a set of differential equations. Expanding the Taylor series for time t in Eq. (2) yields the equivalent formula,

$$\mathbf{q}(\mathbf{r},t) + \sum_{i=1}^{X} \frac{\tau_q^{(i)}}{(i)!} \frac{\partial^{(i)}}{\partial t^{(i)}} \mathbf{q}(\mathbf{r},t) = -\gamma \left\{ \nabla T_a(\mathbf{r},t) + \sum_{j=1}^{Y} \frac{\tau_T^{(j)}}{(j)!} \frac{\partial^{(j)}}{\partial t^{(j)}} [\nabla T_a(\mathbf{r},t)] \right\}, \; X, Y \geq 1, \tag{3}$$

where X and Y determine a progressive interchange between the diffusive and wave-like behaviors [48]. Considering the behavior of thermal waves, we choose the simplest form, that is, $X = Y + 1$. The phase-lags are assumed small, implying that the second-order terms in τ_T and the third-order terms in τ_q and subsequent terms are negligible. In this case, Eq. (3) becomes

$$\mathbf{q}(\mathbf{r},t) + \tau_q \frac{\partial \mathbf{q}(\mathbf{r},t)}{\partial t} + \frac{1}{2}\tau_q{}^2 \frac{\partial^2 \mathbf{q}(\mathbf{r},t)}{\partial t^2} + o(\mathbf{q}) \cong -\gamma \left[\nabla T_a(\mathbf{r},t) + \tau_T \frac{\partial \nabla T_a(\mathbf{r},t)}{\partial t} + o(\nabla T_a) \right], \tag{4}$$

substituting Eq. (4) into Eq. (1) gives

$$\gamma\left[\nabla T_a(\mathbf{r},t)+\tau_T\frac{\partial\nabla T_a(\mathbf{r},t)}{\partial t}\right]=C_p\left[\frac{\partial T_a(\mathbf{r},t)}{\partial t}+\tau_q\frac{\partial^2 T_a(\mathbf{r},t)}{\partial t^2}+\frac{1}{2}{\tau_q}^2\frac{\partial^3 T_a(\mathbf{r},t)}{\partial t^3}\right]. \tag{5}$$

Following Carcione et al. [2], the heat equation in thermoporoelastic media can be written as

$$\gamma\left(\Delta T+\tau_T\Delta\dot{T}\right)=c'\boldsymbol{\tau_q}^{\mathbf{X}=2}\mathbf{A_1}+T_0\beta\left[\boldsymbol{\tau_q}^{\mathbf{X}=2}(\mathbf{A_2}+\mathbf{A_3})\right]+S, \tag{6}$$

where $\boldsymbol{\tau_q}^{\mathbf{X}=2}=\left[1,\tau_q,\frac{1}{2}{\tau_q}^2\right]^{\mathrm{T}}$, $\mathbf{A_i}=\left[\dot{A}_i,\ddot{A}_i,\dddot{A}_i\right]$, $i=1,2,3$ correspond to T, ε_m, ε_f respectively, c' is the bulk specific heat of the unit volume in the absence of deformation, β is the coefficient of thermal stress, Δ is the Laplacian operator, and the dot above a variable denotes time differentiation, T is the increment of temperature over a reference T_0, ε_m and ε_f are the solid and fluid strain, respectively. In the following, the subscripts "m" and "f" refer to the solid (dry) frame and fluid, respectively.

2.2. Governing equations

The stress-strain constitutive relations in the dynamical thermoporoelastic medium are [1, 22]

$$\begin{cases}\sigma_{ij}=\lambda\delta_{ij}u_{k,k}+\mu(u_{i,j}+u_{j,i})+\alpha M\delta_{ij}(\alpha u_{k,k}+w_{k,k})-\beta\delta_{ij}T+f_m\\ \sigma_f=-\phi p=\phi M(\alpha u_{k,k}+w_{k,k})-\beta_f T+f_f\end{cases}, \tag{7}$$

where σ_{ij} and σ_f are the stress components of the frame and fluid, respectively, p is the fluid pressure, λ and μ are the dry-rock Láme constants, δ_{ij} is the Kronecker-delta, u_i is the displacement components of the frame, ϕ is the porosity, and f are external sources.

The elastic coefficients in Eq. (7) are

$$\begin{cases}\alpha=1-\dfrac{K_m}{K_s},K_m=\lambda+\dfrac{2}{3}\mu,\beta=\beta_s+\phi\beta_f\\ M=\dfrac{K_s}{1-\phi-\frac{K_m}{K_s}+\phi\frac{K_s}{K_f}},w_i=\phi(c_i-u_i)\end{cases}, \tag{8}$$

where K is the bulk moduli, and c_i are the displacement components of the fluid.

The dynamic equations are

$$\begin{cases}\sigma_{ij,j}=\rho\ddot{u}_i+\rho_f\ddot{w}_i+f_m\\ (-p)_{,i}=\rho_f\ddot{u}_i+m\ddot{w}_i+\dfrac{\eta}{\kappa}\dot{w}_i+f_f\\ \gamma\left(T_{,ii}+\tau_T\dot{T}_{,ii}\right)=\rho C_e\boldsymbol{\tau_q}^{\mathbf{X}=2}\mathbf{A_1}+\beta T_0\left[\boldsymbol{\tau_q}^{\mathbf{X}=2}(\mathbf{U}+\mathbf{W})\right]+S\end{cases}, \tag{9}$$

with

$$\begin{cases}\rho=(1-\phi)\rho_s+\phi\rho_f\\ m=\dfrac{\varsigma\rho_f}{\phi}\end{cases}, \tag{10}$$

where ρ is the density, ς is the tortuosity, η is the fluid viscosity, κ is the frame permeability, C_e is the specific heat capacity, $\mathbf{U}=[\dot{u}_{i,i},\ddot{u}_{i,i},\ddot{u}_{i,i}]$ and $\mathbf{W}=[\dot{w}_{i,i},\ddot{w}_{i,i},\ddot{w}_{i,i}]$. The effect of microscopic interactions vanishes when the double-phase coupling approaches infinity, implying that both phase-lags τ_q and τ_T (macroscopic) approach zero. Equation (5) reduces to the classical diffusion equation in this case and the assumption of instantaneous thermodynamic equilibrium is retrieved.

Substituting the constitutive relations (7) into the dynamical equations (9), we obtain the following compact equations describing the coupling between the displacement components and

temperature fluctuations,

$$\begin{cases} \left(\lambda+\mu+\alpha^2 M\right)u_{j,ij}+\mu u_{i,jj}+\alpha M w_{j,ij}-\beta T_{,i}=\rho\ddot{u}_i+\rho_f\ddot{w}_i \\ M(\alpha u_{j,ij}+w_{j,ij})-\dfrac{\beta_f}{\phi}T_{,i}=\rho_f\ddot{u}_i+m\ddot{w}_i+\dfrac{\eta}{\kappa}\dot{w}_i \\ \gamma\left(T_{,ii}+\tau_T\dot{T}_{,ii}\right)=\rho C_e\boldsymbol{\tau}_{\mathbf{q}}{}^{\mathbf{X}=2}\mathbf{A_1}+\beta T_0\left[\boldsymbol{\tau}_{\mathbf{q}}{}^{\mathbf{X}=2}(\mathbf{U}+\mathbf{W})\right]+S \end{cases}. \tag{11}$$

The coupling of heat and strain only involves volume strains due to the dynamic equations (9). Only one mechanism is considered for the displacement-temperature interaction, that is, the expansion-contraction propagation of P waves induces a dissipative decaying T-wave mode, which is an experimentally confirmed heat-wave interaction mechanism [12]. A plane-wave analysis to obtain the phase velocity and attenuation factor of the wave modes is given in Appendix A.

3. Particle velocity-stress-temperature formulation

We consider the (x,z)-plane and solve the differential equations by using a first-order approach in time, called particle velocity-stress-temperature formulation in elasticity. We recast the equations as new expressions to be used for numerical simulations. Eq. (7) become

$$\begin{cases} \dot{v}_x=\beta_{11}(\partial_x\sigma_{xx}+\partial_z\sigma_{xz}-f_x)-\beta_{12}\left(\partial_x p+\dfrac{\eta}{\kappa}q_x\right)\equiv\Pi_x \\ \dot{v}_z=\beta_{11}(\partial_x\sigma_{xz}+\partial_z\sigma_{zz}-f_z)-\beta_{12}\left(\partial_z p+\dfrac{\eta}{\kappa}q_z\right)\equiv\Pi_z \\ \dot{q}_x=\beta_{21}(\partial_x\sigma_{xx}+\partial_z\sigma_{xz}-f_x)-\beta_{22}\left(\partial_x p+\dfrac{\eta}{\kappa}q_x\right)\equiv\Omega_x \\ \dot{q}_z=\beta_{21}(\partial_x\sigma_{xz}+\partial_z\sigma_{zz}-f_z)-\beta_{22}\left(\partial_z p+\dfrac{\eta}{\kappa}q_z\right)\equiv\Omega_z \\ \dot{\sigma}_{xx}=(\lambda+2\mu)\partial_x v_x+\lambda\partial_z v_z+\alpha^2 M(\partial_x v_x+\partial_z v_z)+\alpha M(\partial_x q_x+\partial_z q_z)-\beta\psi+\dot{f}_{xx} \\ \dot{\sigma}_{zz}=(\lambda+2\mu)\partial_z v_z+\lambda\partial_x v_x+\alpha^2 M(\partial_x v_x+\partial_z v_z)+\alpha M(\partial_x q_x+\partial_z q_z)-\beta\psi+\dot{f}_{zz} \\ \dot{\sigma}_{xz}=\mu(\partial_x v_x+\partial_z v_z)+\dot{f}_{xz} \\ \dot{p}=-\alpha M(\partial_x v_x+\partial_z v_z)-M(\partial_x q_x+\partial_z q_z)+\dfrac{\beta_f}{\phi}\psi-\dfrac{1}{\phi}\dot{f}_f \end{cases}, \tag{12}$$

with

$$\begin{bmatrix}\beta_{11} & \beta_{12}\\ \beta_{21} & \beta_{22}\end{bmatrix}=\left(\rho_f{}^2-\rho m\right)^{-1}\begin{bmatrix}-m & \rho_f\\ \rho_f & -\rho\end{bmatrix}, \tag{13}$$

where v_i and q_i are the components of the particle velocity fields of the frame and fluid, respectively. We define

$$\dot{T}=\psi,\ \dot{\psi}=H, \tag{14}$$

and Eq. (11_3) yields

$$\dot{H} = \frac{2\gamma}{\rho C_e {\tau_q}^2}\left[\partial_{xx}T + \partial_{zz}T + \tau_T(\partial_{xx}\psi + \partial_{zz}\psi)\right] - \frac{2}{{\tau_q}^2}\left(\psi + \tau_q H\right) - \frac{2S}{\rho C_e {\tau_q}^2} - \frac{2\beta T_0}{\rho C_e {\tau_q}^2}\begin{bmatrix}\partial_x v_x + \partial_z v_z + \partial_x q_x + \partial_z q_z + \tau_q(\partial_x \Pi_x + \partial_z \Pi_z + \partial_x \Omega_x + \partial_z \Omega_z) \\ + \frac{1}{2}{\tau_q}^2(\partial_x \Gamma_x + \partial_z \Gamma_z + \partial_x \Lambda_x + \partial_z \Lambda_z)\end{bmatrix}, \tag{15}$$

with

$$\begin{cases}\Gamma_x = \dot{\Pi}_x, \Gamma_z = \dot{\Pi}_z \\ \Lambda_x = \dot{\Omega}_x, \Lambda_z = \dot{\Omega}_z\end{cases}. \tag{16}$$

Equations (12)–(16) can be written in matrix form as

$$\dot{\mathbf{v}} + \mathbf{s} = \mathbf{M}\mathbf{v}, \tag{17}$$

where

$$\mathbf{v} = [v_x, v_z, q_x, q_z, \sigma_{xx}, \sigma_{zz}, \sigma_{xz}, p, T, \psi, H]^{\mathrm{T}}, \tag{18}$$

is the unknown vector,

$$\mathbf{s} = \left[-\beta_{11}\dot{f}_x, -\beta_{11}\dot{f}_z, -\beta_{21}\dot{f}_x, -\beta_{21}\dot{f}_z, \dot{f}_{xx}, \dot{f}_{zz}, \dot{f}_{xz}, -\frac{\dot{f}_f}{\phi}, 0, S'\right]^{\mathrm{T}}, \tag{19}$$

is the source vector. Matrix $\mathbf{M}$ is the propagation operator derived from Eqs. (12)–(16). The solution to Eq. (17) subject to the initial condition $\mathbf{v}(0) = \mathbf{v}_0$ is formally given by

$$\mathbf{v}(t) = \exp(t\mathbf{M})\mathbf{v}_0 + \int_0^t \exp(\tau\mathbf{M})\mathbf{s}(t-\tau)d\tau, \tag{20}$$

where $\exp(t\mathbf{M})$ is called the evolution operator.

The eigenvalues of $\mathbf{M}$ may have negative real parts and differ greatly in magnitude. The presence of both large and small eigenvalues indicates that the problem is stiff. Moreover, the presence of real positive eigenvalues can induce instability in the time-stepping method. To solve these problems, the differential equations are solved with the splitting algorithm used by Carcione and Quiroga-Goode [49] and Carcione and Seriani [50]. The propagation matrix can be partitioned as

$$\mathbf{M} = \mathbf{M}_r + \mathbf{M}_s, \tag{21}$$

where the subscript r indicates the regular matrix, and the subscript s denotes the stiff matrix, involving the quantity γ and the coupling terms. The evolution operator can be expressed as $\exp(\mathbf{M}_r + \mathbf{M}_s)t$. It is easy to show that

$$\exp(\mathbf{M}dt) = \exp\left(\frac{1}{2}\mathbf{M}_s dt\right)\exp(\mathbf{M}_r dt)\exp\left(\frac{1}{2}\mathbf{M}_s dt\right), \tag{22}$$

has second-order accuracy $\mathrm{O}(dt^2)$. We solve the equations with the time integration method in Appendix B.

4. Results

4.1. Plane-wave analysis

We obtain velocity and attenuation in saturated quartzite using the properties listed in Table 1. The lagging times are $\tau_q = 7.81 \times 10^{-8}$ s and $\tau_T = 4.74 \times 10^{-7}$ s. The calculation of lagging times and thermal properties is discussed in Section 5.2. In addition, we calculated the wave velocity

Table 1. Material properties.

Properties	Values
Shear modulus, μ	8.6 GPa
Density, ρ_s	2640 kg/m^3
Frame bulk modulus, K_m	1.7 GPa
Grain modulus, K_s	7.88 GPa
Water bulk modulus, K_f	2.4 GPa
Porosity, φ	0.3
Permeability, κ	1 Darcy
Tortuosity, ς	2
Water density, ρ_f	1000 kg/m^3
Thermoelasticity coefficient, β_f	40,000 kg/(m s^2 K)
Viscosity, η	0.001 Pa/s
Bulk specific heat capacity, C_e	0.25 m^2 /(s^2 K)
Thermoelasticity coefficient, β	120000 kg/(m s^2 K)
Absolute temperature, T_0	300 K
Thermal conductivity, γ	8.76 m kg/(s^3 K)

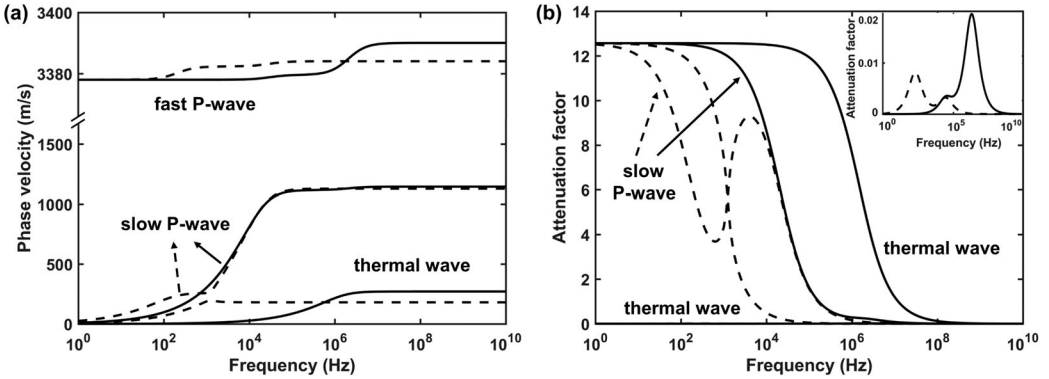

Figure 1. Phase velocity (a) and attenuation factor (b) as a function of frequency for the SPL model. The properties are given in Table 1. The solid line corresponds to saturated quartzite ($\tau_q = 7.81 \times 10^{-8}$ s and $\tau_T = 0$ s), whereas the dashed line corresponds to a synthetic material ($\tau_q = 7.81 \times 10^{-4}$ s and $\tau_T = 0$ s).

for a type of synthetic material. Referring to Carcione et al. [1], we define the value of the thermal conductivity of the hypothetical medium as $\gamma = 8.76 \times 10^4$ m kg/(s^3°K), with a corresponding increase in the lagging times of $\tau_q = 7.81 \times 10^{-4}$ s and $\tau_T = 4.74 \times 10^{-3}$ s. The reason for comparing different materials is to demonstrate the physical behavior associated with different lagging times and thermal properties. As indicated by Eq. (A3), the S wave is independent of the thermal effects because the shear strains are not coupled with the temperature field in homogeneous media. That is, the S wave is not affected by temperature.

Figure 1 shows the frequency-dependent phase velocity and attenuation for the SPL model ($\tau_T = 0$) [1, 22]. The solid and dashed lines correspond to saturated quartzite and a high thermal conductivity synthetic material, respectively. Figure 1(b) shows the fast P-wave attenuation results. We can see that the fast P wave has two Zener-like relaxation peaks, which are related to the Biot and thermal loss mechanisms. Moreover, the thermal and Biot slow waves have similar characteristics, being strongly diffusive at low frequencies. For the synthetic material, the thermal attenuation peak moves to low frequencies.

Figure 2 shows the results for the DPL model. As indicated in Section 5.2, we state that the relationship between the two lagging times in rocks is $\tau_q < \tau_T$. Other properties are the same as in Figure 1 except for the lagging times. Increasing the delay time also shifts the frequency of the thermal attenuation peak to a lower frequency. Figure 2b shows that the characteristic frequency of the thermal wave is reduced by four orders of magnitude. The DPL model is more sensitive to

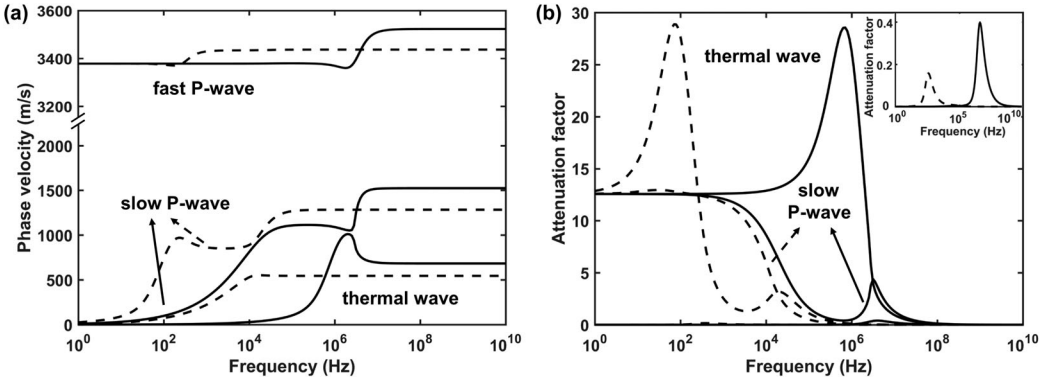

Figure 2. Phase velocity (a) and attenuation factor (b) as a function of frequency for the DPL model. The properties are given in Table 1. The solid line corresponds to saturated quartzite, whereas the dashed line corresponds to a synthetic material.

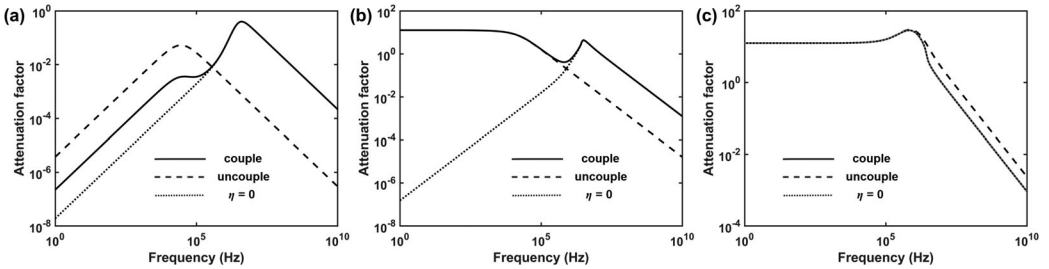

Figure 3. Attenuation factor of the fast P wave (a), slow P wave (b), and thermal wave (c) in the DPL model. The properties are those of saturated quartzite.

changes in thermal properties and delays time than the LS model, which confirms the τ_T physical interpretation. Figure 3 illustrates the effect of the two mechanisms, that is, poroelasticity and thermoelasticity. In the uncoupled case ($\beta = \beta_f = 0$), the attenuation of the P wave (a single peak in the kHz range) is of poroelastic nature. On the other hand, zero viscosity implies that all energy losses are due to thermal effects. Figure 3c shows that the thermal attenuation is independent of the fluid viscosity, with attenuation in the MHz frequencies.

We compare the phase velocity and attenuation of several typical rocks with different frames and fluids. In addition to the lagging times, other model properties related to the fluid and rock frame are changed (see Appendix C). The results are shown in Figures 4 and 5. We observe that:

1. Saturation with different fluids in the same quartzite frame: the results are not only affected by the fluid properties (density, viscosity, etc.), but also by the thermal properties (thermal conductivity, specific heat). When the fluid is gas (air), the limit velocity and velocity variation of the P wave are the largest (Figure 4a,b), and the attenuation frequency range is wider than that of glycerol and water (Figure 4d,e). Figures 4c and f indicate that the T wave velocity and attenuation for glycerin-saturated quartzite are higher. The P wave is more affected by the fluid, while the T wave is by the thermal properties.
2. Different rock frames saturated with water: at relatively low frequencies ($<10^2$ Hz), the velocity and attenuation are the same. Discrepancies occur as frequency increases. This is because the wave properties at high frequencies are dominated by the thermal effects, whereas those at low frequencies are mainly affected by the Biot flow. The fast P-wave velocity dispersion decreases, while the limit velocity increases (Figure 5a). The relaxation frequencies do not change by varying the rock-frame properties.

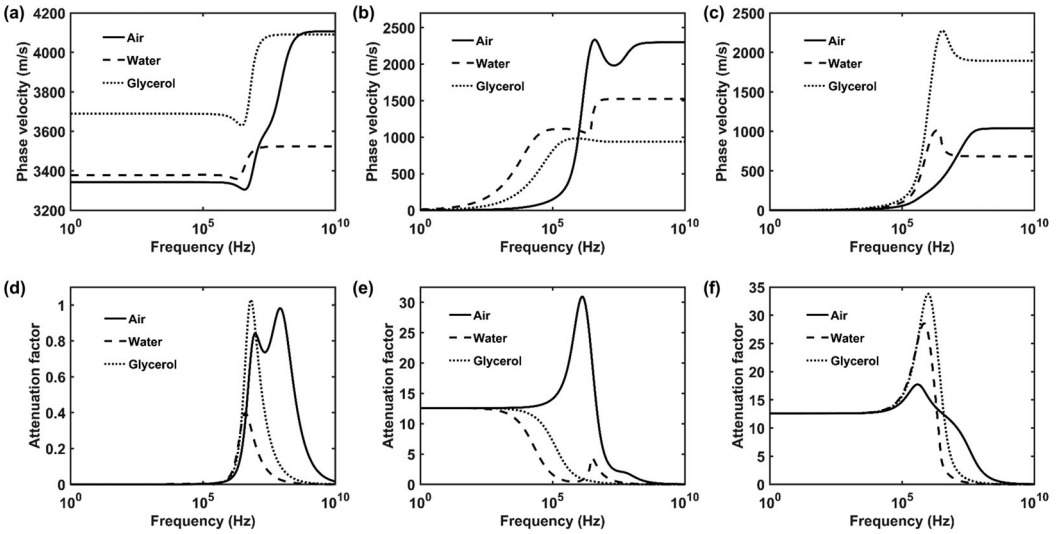

Figure 4. Phase velocity (a–c) and attenuation factor (d–f) of the fast P wave, slow P wave, and T wave correspond to the DPL model. The solid, dashed, and dotted lines correspond to quartzite saturated with air, water, and glycerol, respectively.

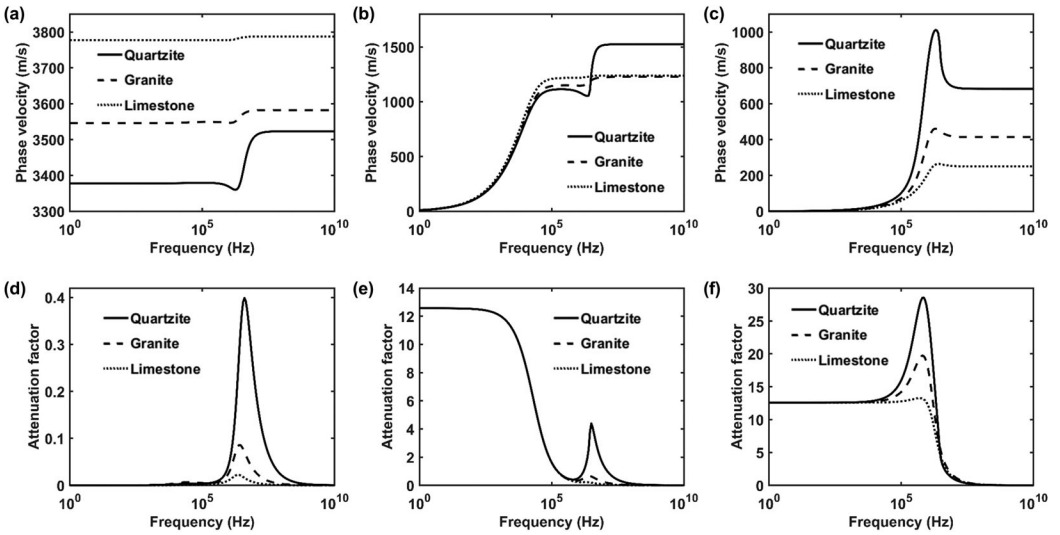

Figure 5. Phase velocity (a–c) and attenuation factor (d–f) of the fast P wave, slow P wave, and T wave correspond to the DPL model. The solid, dashed, and dotted lines correspond to water-saturated quartzite, granite, and limestone, respectively.

3. When the rock is denser and stiffer, there is a rapid energy exchange between the pore infill and the background. The shorter lagging time results in high velocity and low attenuation. The pore-fluid properties affect both the thermal process and the Biot mechanism.

4.2. Simulations

Next, we compute snapshots of the wavefield by using the RSG-FD method, with a mesh of 461×461 grid points. The source is a Ricker wavelet located at the center of the mesh and has the time history

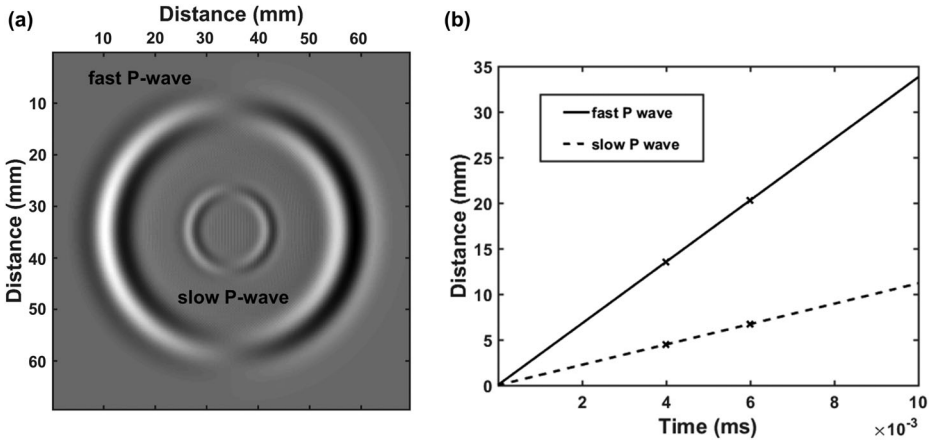

Figure 6. Snapshots of v_x at 6 μs in saturated quartzite and a dilatational stress source (τ_{xx} and τ_{zz}) with a center frequency of 0.6 MHz, corresponding to the solid lines of Figure 1.

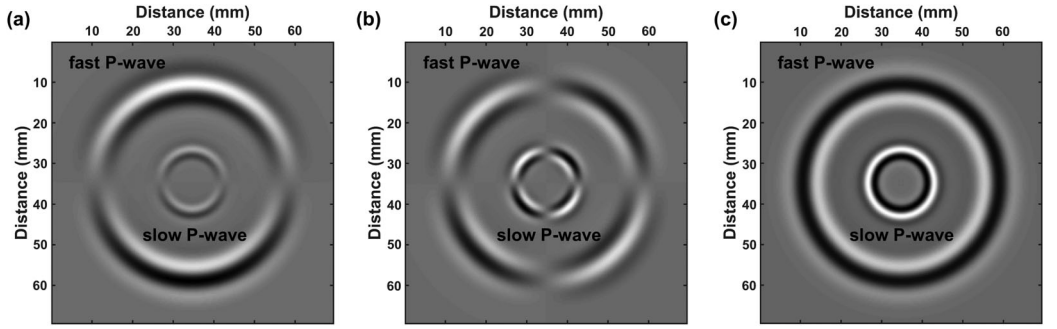

Figure 7. Snapshots of v_z (a), τ_{xz} (b), and T (c) in DPL saturated quartzite, corresponding to the solid lines of Figure 2. The properties are those to produce Figure 6.

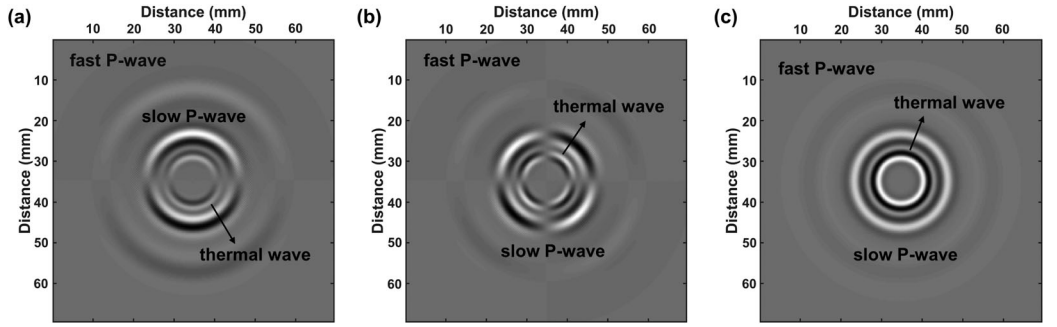

Figure 8. Snapshots of v_z (a), τ_{xz} (b), and T (c) in DPL high thermal conductivity media, corresponding to the dashed lines of Figure 2. The properties are those to produce Figure 6.

$$w(t) = \cos\left[2\pi(t - t_0)f_0\right] \exp\left[-2(t - t_0)^2 {f_0}^2\right], \tag{23}$$

where f_0 is the central frequency, $t_0 = 3/(2f_0)$ is the delay time.

Figure 6a shows a snapshot of the wavefield for saturated quartzite, where we assume a grid spacing of $dx = dz = 0.15$ mm, a time step of $dt = 10$ ns, and a center frequency of 0.6 MHz. Figure 6b shows the correspondence between the plane-wave analysis and the wave velocity extracted from the snapshot. The fast P wave and the slow P wave travel at velocities of 3380 m/s

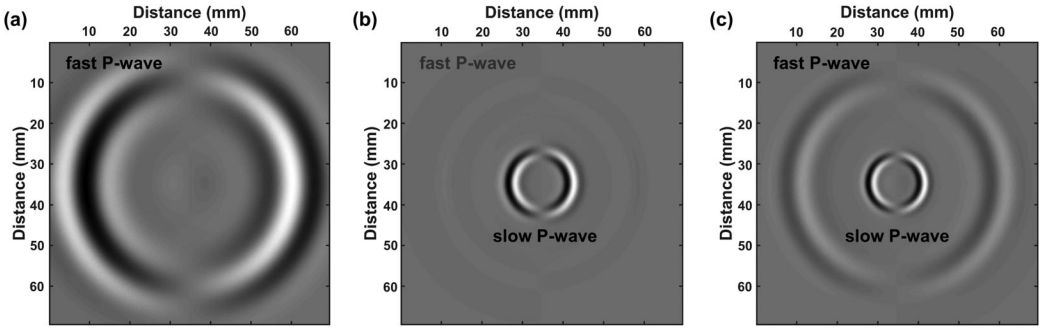

Figure 9. Snapshots of the particle velocity of the fluid q_z in quartzite saturated with air (a), water (b), and glycerol (c). The properties are those to produce Figure 6.

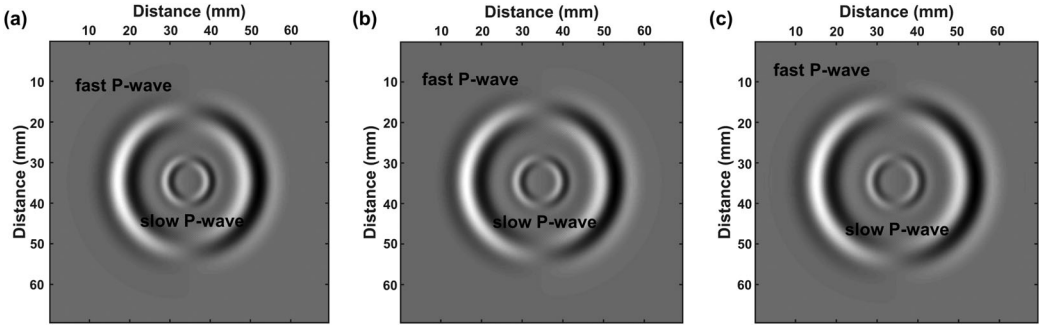

Figure 10. Snapshots of the particle velocity of the solid v_x at 5 μs in saturated quartzite (a), granite (b), and limestone (c). The properties are those to produce Figure 6.

and 1118 m/s, respectively, corresponding to the two waveforms in the snapshot. The T wave is diffusive due to a high value of the attenuation factor at the source frequency band.

Figure 7 shows v_z, τ_{xz}, and T snapshots of DPL saturated quartzite (Figure 2). The fast and slow P-wave velocities are less than the limit velocity, which are 3375 m/s and 1106 m/s respectively. Figure 8 shows similar snapshots for high thermal conductivity media, corresponding to the dashed lines in Figure 2. Increasing the lagging time results in a significant decrease in the attenuation factor and peak frequency so that the T wave is wave-like. According to the stress-strain relationships, if β is equal to zero, the waves become uncoupled.

Figure 9 compares snapshots of the fluid particle velocity q_z for quartzite saturated with different fluids. The attenuation of the fast P-wave is the lowest in the case of gas. According to Figure 4f, the extreme attenuation causes the diffusion-like character of the T and Biot (slow) waves (Figure 9a). Furthermore, the slow P-wave velocity for water saturation is higher than that for glycerol. Snapshots of the solid particle velocities v_x for different frames saturated with water are shown in Figure 10. The P-wave velocity is higher for limestone and lower for quartzite, and the same behavior can be observed in the simulations.

Finally, we present an example of wave propagation in inhomogeneous media. We consider a three-layer medium, where the properties of the upper and lower half spaces are the same. In Figure 11a, the upper and lower half spaces are water-saturated quartzite, and the middle layer is glycerin-saturated quartzite. The wave velocity in the middle layer is the higher one. On the other hand, in Figure 11b the velocity of this layer is lower because the upper and lower half spaces are water-saturated limestone. Figure 11c corresponds to water-saturated-quartzite half spaces, and the middle layer has a high thermal conductivity (water-saturated synthetic medium). Other

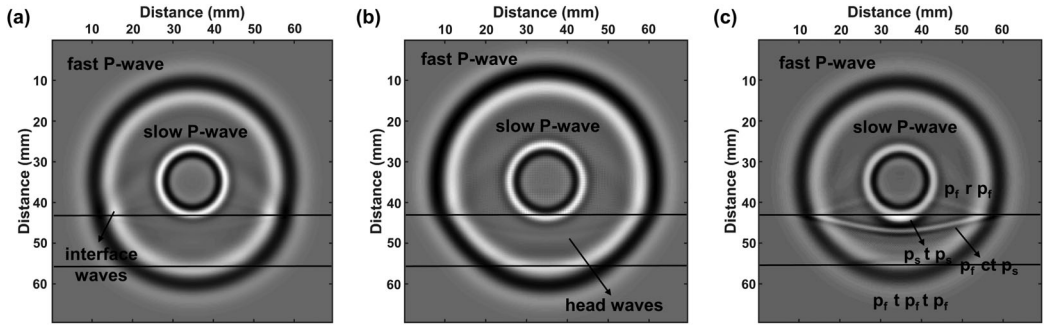

Figure 11. Temperature snapshots in a three-layer medium. The upper and lower half-spaces have the same properties. The labels indicate the fast P wave (P_f), slow P wave (P_s), direct reflected (r), converted (c), and transmitted (t) waves. The properties are those to produce Figure 6.

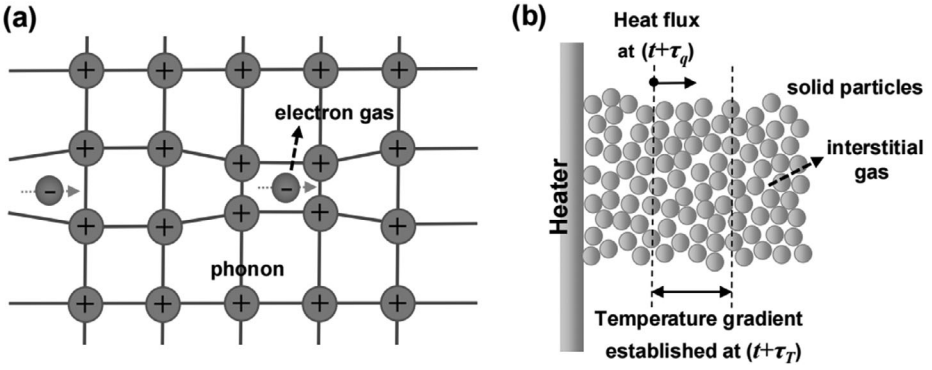

Figure 12. Different delay behaviors in (a) metal thin layer and (b) sand bed.

properties are those produced in Figure 6. The snapshots are computed at 6 μs, and show reflected, transmitted, and converted-transmitted waves, denoted by *r*, *t*, and *ct*.

5. Discussion

5.1. Physical meaning of the lagging times in metals and sand

In this section, we compare the DPL model with the microscopic two-step model and discuss the physical meaning of the lagging times in rocks based on the experimental results of thin metal layers and sand beds. The thermal response time and the phonon-electron lagging time are characteristics of thin metal layers. The two-step model proposes that the energy exchange between microscopic particles must be considered in describing the thermal behavior, as shown in Figure 12a.

The double lagging times of the DPL theory are derived in analogy with the two-step model. Equation (2) of Qiu and Tien [34] accounting for microscopic interactions has the same form as Eqs. (4) and (5) of Tzou [35] employing the macroscopic DPL concept. The macro representation of the lagging times is

$$\tau_q = \frac{\alpha_E}{V_{T0}{}^2}, \tau_T = \frac{\alpha_e}{V_{T0}{}^2}, \tag{24}$$

where α_E is the equivalent thermal diffusivity of the medium, V_{T0} is the T-wave velocity, and α_e is the electron diffusivity in the metal. The lagging time of the heat-flux vector (τ_q) captures the

thermal wave behavior, the equivalent time-delay response of the medium as a whole, while the lagging time of the TG (τ_T) captures the effect of the electron gas on the lattice, the response of the microscale interaction. Experiments in several metals confirmed the above point [34, 51, 52]), taking Cu as an example $\tau_T = 70.833\,\text{ps}$ and $\tau_q = 0.4348\,\text{ps}$, differ by two orders of magnitude. In addition, the simulations based on the DPL model better describe the thermal waves observed in superfluid liquid helium [35].

To further emphasize the correspondence between lagging time and microstructure, Tzou [46] used the DPL model to describe thermal lagging in sands, as illustrated in Figure 12b. In analogy with phonons and electrons in metals, the solid and gas phases are treated as different energy carriers. The physical mechanisms are different, but the analogy of microstructural interaction in space with the fast-transient effect in time is similar. The τ_T is regarded as the lagging time of the pore infill, which is proportional to the thermal diffusivity of the fluid. The transient experiment confirms that the DPL model smoothes the sharp wavefronts of the CV theory in describing heat transfer in porous materials, which is shown in Figures 6.6 and 6.14 of Tzou [46]. More detailed analysis and experiments also discuss the lagging response in porous media [53, 54].

5.2. Application of the DPL theory to rocks

In the thermoelastic theory, heat conduction is described by the CV equation. The introduction of the lagging time τ_q leads to the finiteness of the thermal wave velocity. However, the pore infill induces energy exchange at the microscopic spatial scale. Our interpretation is that the heat-flux lagging time τ_q represents the macroscopic effect of the bulk rock and the TG lagging time τ_T embodies the microscopic effect of the fluid phase.

Regarding τ_q, Carcione et al. [2] calculated the CV delay time according to the Rudgers [8] lattice model. When considering the limit case in thermoelasticity, the two (P and T) waves can be completely uncoupled, and both will attain the same limit velocity. Thus, the lagging time τ_q can be calculated by substituting the P-wave velocity for the T-wave velocity. We replace V_{T0} in Eq. (A7) with the P-wave velocity, $V_{P0} = \sqrt{\frac{\lambda+2\mu}{\rho}} = 2457\text{m/s}$, and then obtain the value of the heat-flux lagging time $\tau_q = \frac{\alpha_E}{{V_{T0}}^2} = \frac{\gamma}{c'{V_{P0}}^2} = 1.49 \times 10^{-8}\text{s}$ [2]. Implicit in the theory is the fact that heat is transported by elastic waves, and it follows that the maximum T-wave velocity is lower than the velocity at which an elastic disturbance propagates in the medium. Moreover, the form of τ_q in the DPL theory is exactly the same as Eq. (24), and the equivalent thermal diffusivity is related to the specific heat capacity and thermal conductivity in two-phase porous media

$$\alpha_E = \frac{c'_m + c'_f}{\gamma_m + \gamma_f}. \tag{25}$$

The lagging time is

$$\tau_q = \frac{\alpha_E}{{V_{P0}}^2}. \tag{26}$$

Regarding τ_T, α_e in Eq. (24) corresponds to the thermal diffusivity of the fluid in a thermoporoelastic medium. But since the mineral grains in actual rocks are much smaller than the sand particles, a uniform temperature distribution is established instantly when heat flows.

According to the modified formula of Eq. (6.18) in Tzou [46], τ_T is

$$\tau_T = \frac{\alpha_m + \alpha_f}{{V_{P0}}^2}, \tag{27}$$

with

Table 2. Thermal properties of different materials.

Substance	T_0 [°K]	ρ [Mg/m^3]	K [GPa]	c' [J/(g°K)]	γ [W/(m°K)]	β [10^{-5}°K^{-1}]
Copper	298.15	8.933	139.0	0.3847	386.0	5.01
Lead	298.15	11.34	36.6	0.1276	35.0	8.67
Limestone	300	2.71	76.0	2.28	3.85	0.339
Quartzite	300	2.64	42.0	1.98	8.16	0.108
Granite	300	2.65	46.0	1.56	–	0.78
Water	298.15	0.997	2.23	4.18	0.60	23.37
Glycerol	298.15	1.26	4.64	2.38	0.29	50.50
Water	554	0.773	0.0055	3.89	0.59	219.9
Helium	298.15	0.00016	0.00016	5.1975	0.15	365.9
Air	298.15	0.0012	0.00014	1.0045	0.024	367.90

$$\alpha_m = \frac{\gamma_m}{c'_m}, \alpha_f = \frac{\gamma_f}{c'_f}. \tag{28}$$

The values of τ_T and τ_q are calculated according to the above Eqs. (25)–(28) and experimental data of Rudgers [8], Kjartansson [55], and Carcione et al. [1, 2]. The properties are shown in Table 2. We assume that the reference velocity of the saturated quartzite is 3000 m/s. The lagging times are $\tau_q = 7.81 \times 10^{-8}$ s and $\tau_T = 4.73 \times 10^{-7}$ s. The range of wave velocity in the rocks is in the order of 10^3 m/s, but the velocity has no effect on the relationship between the two lagging times. By comparing the thermal properties of solid and fluid, we find that the two lagging times are always $\tau_T > \tau_q$ for rocks. That is, the pore fluid takes more time to reach the final thermal equilibrium.

6. Conclusions

We combine the DPL model and thermoporoelasticity to develop a DPL theory for wave propagation in porous media, considering the dissimilar thermal relaxations between the frame and the fluid phase. This implies two lagging times: the heat-flux lagging time τ_q for the macroscopic effect of the whole rock, and the TG lagging time τ_T corresponding to the microscopic effect of the fluid phase. Compared to the SPL theory, the DPL model predicts higher attenuation and limit velocity. The introduction of the additional lagging time implies that the relaxation peak moves to lower frequencies as the lagging time increases. The plane-wave analysis shows how the solid and fluid phases affect the velocity and attenuation of the elastic and thermal waves. The lagging time determines the diffusion length of the heat and fluid flows, dominating the inelastic thermal effects at high frequencies, but barely influencing the wave features in the seismic frequency band. Finally, we develop a FD algorithm to solve the DPL thermoporoelastic equations. A time-splitting algorithm overcomes instability problems. The theory can be used to explain experimental data, especially for porous rocks containing organic inclusions associated with thermoviscoelasticity and thermal-relaxation mechanisms.

APPENDIX A: plane-wave analysis

To examine the characteristics of wave propagation in thermoporoelastic media, we consider the following homogeneous plane-wave expressions,

$$\begin{cases} u_i = As_i \exp\left[-i\omega\left(t - \dfrac{l_j}{v_c}x_j\right)\right] \\ w_i = Bd_i \exp\left[-i\omega\left(t - \dfrac{l_j}{v_c}x_j\right)\right] \\ T = C \exp\left[-i\omega\left(t - \dfrac{l_j}{v_c}x_j\right)\right] \end{cases}, \tag{A1}$$

where s_i and d_i are the solid and fluid polarizations, respectively, A, B, and C are amplitude constants, ω is the angular frequency, v_c is the complex velocity, l_j denotes the propagation directions, x_j are the position components, and $i = \sqrt{-1}$.

Substituting Eq. (A1) into Eq. (11) yields a system of algebraic equations,

$$\begin{cases} \left(\lambda+\mu+\alpha^2 M\right)\left(\frac{\omega}{v_c}\right)^2 As_j l_j l_i + \mu\left(\frac{\omega}{v_c}\right)^2 As_i + \alpha M\left(\frac{\omega}{v_c}\right)^2 Bd_j l_j l_i - i\beta\frac{\omega}{v_c}Cl_i = \rho\omega^2 As_i + \rho_f\omega^2 Bd_i \\ M\left[\alpha\left(\frac{\omega}{v_c}\right)^2 As_j l_j l_i + \left(\frac{\omega}{v_c}\right)^2 Bd_j l_j l_i\right] - i\frac{\beta_f}{\phi}\frac{\omega}{v_c}Cl_i = \rho_f\omega^2 As_i + m\omega^2 Bd_i - i\frac{\eta}{\kappa}\omega Bd_i \\ -\gamma\left[\left(\frac{\omega}{v_c}\right)^2 C + i\tau_T\omega\left(\frac{\omega}{v_c}\right)^2 C\right] = \rho C_e\left(i\omega C - \tau_q\omega^2 C - \frac{1}{2}{\tau_q}^2 i\omega^3 C\right) + \\ \beta T_0\left[\left(\frac{\omega}{v_c}\omega As_i l_i + \frac{\omega}{v_c}\omega Bd_i l_i\right) + \tau_q\left(i\frac{\omega}{v_c}\omega^2 As_i l_i + i\frac{\omega}{v_c}\omega^2 Bd_i l_i\right) - \frac{1}{2}{\tau_q}^2\left(\frac{\omega}{v_c}\omega^3 As_i l_i + \frac{\omega}{v_c}\omega^3 Bd_i l_i\right)\right] \end{cases}. \tag{A2}$$

For S waves, $s_i l_i = d_i l_i = 0$, and since the propagation direction is perpendicular to the displacement vector, we have

$$v_c(\text{Swave}) = \sqrt{\frac{\mu}{\rho - \frac{\rho_f}{\frac{\gamma}{\phi} - i\frac{\eta}{\kappa\omega\rho_f}}}}. \tag{A3}$$

We see that the S-wave propagation is independent of the thermal properties in isotropic homogeneous media.

For P waves, $s_i l_i = d_i l_i = 1$, and the propagation direction is parallel to the displacement vector. The dispersion relation is

$$a\left({v_c}^2\right)^3 + b\left({v_c}^2\right)^2 + c{v_c}^2 + d = 0, \tag{A4}$$

where

$$\begin{cases} a = \rho C_e\phi N\left(1+\frac{1}{2}\tau_q i\omega\right)\left(\omega L - i\frac{\eta}{\kappa}\rho\right) \\ b = i\phi\frac{\eta}{\kappa}K - \omega\left\{\frac{\eta}{\kappa}\phi\left[(\gamma + i\gamma\tau_T\omega)\rho + \tau_q\left(1+\frac{1}{2}\tau_q i\omega\right)K\right] + \phi\rho C_e H + T_0\beta J\right\} \\ -i\omega^2\left\{\phi\left[(\gamma + i\gamma\tau_T\omega)L + \rho C_e H\tau_q\left(1+\frac{1}{2}\tau_q i\omega\right)\right] + T_0\beta J\tau_q\left(1+\frac{1}{2}\tau_q i\omega\right)\right\} \\ c = \omega\left\{\phi\left[\rho C_e ME + \frac{\eta}{\kappa}(\gamma + i\gamma\tau_T\omega)F\right] + T_0\beta G\right\} \\ +i\omega^2\left\{\phi\left[(\gamma + i\gamma\tau_T\omega)H + \rho C_e ME\tau_q\left(1+\frac{1}{2}\tau_q i\omega\right)\right] + T_0\beta G\tau_q\left(1+\frac{1}{2}\tau_q i\omega\right)\right\} \\ d = -i\omega^2(\gamma + i\gamma\tau_T\omega)\phi ME \end{cases}, \tag{A5}$$

with

$$\begin{cases} E = \lambda + 2\mu, F = E + \alpha^2 M, G = E\beta_f + M(\alpha - 1)\left(\alpha\beta_f - \phi\beta\right) \\ H = mF + \rho M - 2\alpha M\rho_f, J = \beta_f(\rho - \rho_f) + \phi\beta(m - \rho_f), K = \rho C_e F + T_0\beta^2 \\ L = m\rho - {\rho_f}^2, N = 1 + i\omega\tau_q \end{cases}. \tag{A6}$$

The phase velocity and attenuation factor of the P waves are

$$v_p = \left[\text{Re}\left(\frac{1}{v_c}\right)\right]^{-1}, A = -\omega\text{Im}\left(\frac{1}{v_c}\right). \tag{A7}$$

Deresiewicz [6] introduced another attenuation coefficient, more akin to the dissipation factor (inverse of the Q factor), namely,

$$L = 4\pi\frac{Av_p}{\omega}. \tag{A8}$$

APPENDIX B: Splitting algorithm

We solve the differential equations with a time-splitting algorithm. Equation (19) allows us to solve the unstable equations separately. The time integration from t to $t + dt$ for the stiff matrix $\mathbf{M}_s$ is solved to obtain the intermediate solution from Eqs. (12)–(16). These are

$$\begin{cases} \dot{v}_x = -\dfrac{\eta}{\kappa}\beta_{12}q_x, \dot{v}_z = -\dfrac{\eta}{\kappa}\beta_{12}q_z \\ \dot{q}_x = -\dfrac{\eta}{\kappa}\beta_{22}q_x, \dot{q}_z = -\dfrac{\eta}{\kappa}\beta_{22}q_z \\ \dot{\sigma}_{xx} = -\beta\psi, \dot{\sigma}_{zz} = -\beta\psi\square\phi\dot{p} = \beta_f\psi, \dot{H} = -\dfrac{2}{{\tau_q}^2}\psi - \dfrac{2}{\tau_q}H \end{cases}. \tag{B1}$$

We obtain

$$\begin{cases} v_x* = {v_x}^n + \dfrac{\beta_{12}}{\beta_{22}}\left[\exp\left(-\dfrac{\eta}{\kappa}\beta_{22}dt\right) - 1\right]{q_x}^n, v_z* = {v_z}^n + \dfrac{\beta_{12}}{\beta_{22}}\left[\exp\left(-\dfrac{\eta}{\kappa}\beta_{22}dt\right) - 1\right]{q_z}^n \\ q_x* = \exp\left(-\dfrac{\eta}{\kappa}\beta_{22}dt\right){q_x}^n, q_z* = \exp\left(-\dfrac{\eta}{\kappa}\beta_{22}dt\right){q_z}^n \\ \sigma_{xx}* = {\sigma_{xx}}^n + \dfrac{1}{2}\tau_q\beta\left[\exp\left(-\dfrac{dt}{\tau_q}\right)\left(\cos\dfrac{dt}{\tau_q} + \sin\dfrac{dt}{\tau_q}\right) - 1\right]\psi^n \\ \sigma_{zz}* = {\sigma_{zz}}^n + \dfrac{1}{2}\tau_q\beta\left[\exp\left(-\dfrac{dt}{\tau_q}\right)\left(\cos\dfrac{dt}{\tau_q} + \sin\dfrac{dt}{\tau_q}\right) - 1\right]\psi^n \\ p* = p^n - \dfrac{\tau_q\beta_f}{2\phi}\left[\exp\left(-\dfrac{dt}{\tau_q}\right)\left(\cos\dfrac{dt}{\tau_q} + \sin\dfrac{dt}{\tau_q}\right) - 1\right]\psi^n \\ \psi* = \exp\left(-\dfrac{dt}{\tau_q}\right)\left(\cos\dfrac{dt}{\tau_q} + \sin\dfrac{dt}{\tau_q}\right)\psi^n \end{cases}. \tag{B2}$$

We use the time-splitting algorithm of Carcione et al. [2]. Discretizing time as $t = ndt$, yields

$$\begin{cases} {v_x}^{n+1} = v_x* + dt\left[\beta_{11}(\partial_x\sigma_{xx}* + \partial_z{\sigma_{xz}}^n) - \beta_{12}\left(\partial_x p* + \dfrac{\eta}{\kappa}q_x*\right)\right] \\ {v_z}^{n+1} = v_z* + dt\left[\beta_{11}(\partial_x{\sigma_{xz}}^n + \partial_z\sigma_{zz}*) - \beta_{12}\left(\partial_z p* + \dfrac{\eta}{\kappa}q_z*\right)\right] \\ {q_x}^{n+1} = q_x* + dt\left[\beta_{21}(\partial_x\sigma_{xx}* + \partial_z{\sigma_{xz}}^n) - \beta_{22}\left(\partial_x p* + \dfrac{\eta}{\kappa}q_x*\right)\right] \\ {q_z}^{n+1} = q_z* + dt\left[\beta_{21}(\partial_x{\sigma_{xz}}^n + \partial_z\sigma_{zz}*) - \beta_{22}\left(\partial_z p* + \dfrac{\eta}{\kappa}q_z*\right)\right] \\ {\sigma_{xx}}^{n+1} = \sigma_{xx}* + dt\left[(\lambda + 2\mu)\partial_x v_x* + \lambda\partial_z v_z* + \alpha^2 M(\partial_x v_x* + \partial_z v_z*) + \alpha M(\partial_x q_x* + \partial_z q_z*) - \beta\psi*\right] \\ {\sigma_{zz}}^{n+1} = \sigma_{zz}* + dt\left[(\lambda + 2\mu)\partial_z v_z* + \lambda\partial_x v_x* + \alpha^2 M(\partial_x v_x* + \partial_z v_z*) + \alpha M(\partial_x q_x* + \partial_z q_z*) - \beta\psi*\right] \\ {\sigma_{xz}}^{n+1} = {\sigma_{xz}}^n + dt[\mu(\partial_x v_x* + \partial_z v_z*)] \\ p^{n+1} = p* + dt\left[-\alpha M(\partial_x v_x* + \partial_z v_z*) - M(\partial_x q_x* + \partial_z q_z*) + \dfrac{\beta_f}{\phi}\psi*\right] \\ T^{n+1} = T^n + dt(\psi*) \\ \psi^{n+1} = \psi* + dt(H^n) \\ H^{n+1} = H^n + dt\left\{\begin{array}{c} \dfrac{2\gamma}{\rho C_e{\tau_q}^2}[\partial_{xx}T^n + \partial_{zz}T^n + \tau_T(\partial_{xx}\psi* + \partial_{zz}\psi*)] - \dfrac{2}{\tau_q}H^n - \dfrac{2}{{\tau_q}^2}\psi* - \dfrac{2S}{\rho C_e{\tau_q}^2} \\ -\dfrac{2\beta T_0}{\rho C_e{\tau_q}^2}\left[\begin{array}{c} \partial_x v_x* + \partial_z v_z* + \partial_x q_x* + \partial_z q_z* \\ +\tau_q(\partial_x\Pi_x* + \partial_z\Pi_z* + \partial_x\Omega_x* + \partial_z\Omega_z*) \\ +\dfrac{1}{2}{\tau_q}^2(\partial_x\Gamma_x* + \partial_z\Gamma_z* + \partial_x\Lambda_x* + \partial_z\Lambda_z*) \end{array}\right] \end{array}\right\} \end{cases}, \tag{B3}$$

where

$$\begin{cases} \Gamma_x* = \beta_{11}\left(\partial_x \dot{\sigma}_{xx}* + \partial_z \dot{\sigma}_{xz}{}^n\right) - \beta_{12}\left(\partial_x \dot{p}* + \dfrac{\eta}{\kappa}\dot{q}_x*\right) \\ \Gamma_z* = \beta_{11}\left(\partial_x \dot{\sigma}_{xz}{}^n + \partial_z \dot{\sigma}_{zz}*\right) - \beta_{12}\left(\partial_z \dot{p}* + \dfrac{\eta}{\kappa}\dot{q}_z*\right) \\ \Lambda_x* = \beta_{21}\left(\partial_x \dot{\sigma}_{xx}* + \partial_z \dot{\sigma}_{xz}{}^n\right) - \beta_{22}\left(\partial_x \dot{p}* + \dfrac{\eta}{\kappa}\dot{q}_x*\right) \\ \Lambda_z* = \beta_{21}\left(\partial_x \dot{\sigma}_{xz}{}^n + \partial_z \dot{\sigma}_{zz}*\right) - \beta_{22}\left(\partial_z \dot{p}* + \dfrac{\eta}{\kappa}\dot{q}_z*\right) \end{cases}, \tag{B4}$$

where eighth- and second-order FD approximations are used for the space and time derivatives, respectively. The variables indicated with an asterisk correspond to the intermediate solutions at each time step.

APPENDIX C: Properties setting

In Figures 4 and 5, we plot the results of the plane-wave analysis for different fluids and frames. The properties of quartzite for different saturating fluids are shown in Table C1, and the properties of different frames are shown in Table C2. Non-listed units are those of Table 1.

Table C1. Properties of quartzite saturated by different fluids.

Properties	Values (Air/water/glycerol)
Water bulk modulus, K_f	0.14/2.4/8.5
Permeability, κ	0.001/1/100
Water density, ρ_f	100/1000/1260
Thermoelasticity coefficient, β_f	80,000/40,000/20,000
Viscosity, η	0.00001/0.001/0.8
Bulk specific heat capacity, C_e	0.12/0.25/0.18
Thermal conductivity, γ	8.18/8.76/8.45
Reference velocity, V_{p0}	2700/3000/3200

Table C2. Properties of different rock frames.

Properties	Values (quartzite/granite/limestone)
Shear modulus, μ	8.6/8.8/10.5
Density, ρ_s	2640/2650/2710
Frame bulk modulus, K_m	1.7/2.0/2.9
Grain modulus, K_s	7.88/8.1/8.6
Bulk specific heat capacity, C_e	0.25/0.23/0.26
Thermoelasticity coefficient, β	120,000/130,000/150,000
Thermal conductivity, γ	8.76/5.28/4.45
Reference velocity, V_{p0}	3000/3200/3700

Disclosure statement

No potential conflict of interest was reported by the author(s).

Funding

The research is supported by the National Natural Science Foundation of China (Grant Nos. 42230803, 41821002); and 111 project "Deep-Superdeep Oil & Gas Geophysical Exploration" (B18055).

Data availability statement

The code and data relating to this work are available, and will be shared on reasonable request to the corresponding author.

References

[1] J. M. Carcione, F. Cavallini, E. J. Wang, J. Ba, and L. Y. Fu, "Physics and simulation of wave propagation in linear thermo-poroelastic media," *J. Geophys. Res.*, vol. 124, no. 8, pp. 8147–8166, 2019.

[2] J. M. Carcione, Z. W. Wang, W. Ling, E. Salusti, J. Ba, and L. Y. Fu, "Simulation of wave propagation in linear thermoelastic media," *Geophysics*, vol. 84, no. 1, pp. T1–T11, 2018.

[3] J. M. Carcione, *Wave Fields in Real Media: Theory and Numerical simulation of Wave Propagation in Anisotropic, Anelastic, Porous and Electromagnetic Media*, 4th ed. New York: Elsevier, 2022.

[4] M. A. Biot, "Thermoelasticity and irreversible thermodynamics," *J. Appl. Phys.*, vol. 27, no. 3, pp. 240–253, 1956.

[5] M. A. Biot, "The theory of propagation of elastic waves in a fluid-saturated porous solid—I. Low-frequency range II. Higher frequency range," *J. Acoust. Soc. Am.*, vol. 28, no. 2, pp. 168–191, 1956.

[6] H. Deresiewicz, "Plane waves in a thermoelastic solid," *J. Acoust. Soc. Am.*, vol. 29, no. 2, pp. 204–209, 1957.

[7] H. W. Lord and Y. Shulman, "A generalized dynamical theory of thermoelasticity," *J. Mech. Phys. Solids*, vol. 15, no. 5, pp. 299–309, 1967.

[8] A. J. Rudgers, "Analysis of thermoacoustic wave propagation in elastic media," *J. Acoust. Soc. Am.*, vol. 88, no. 2, pp. 1078–1094, 1990.

[9] M. D. Sharma, "Wave propagation in thermoelastic saturated porous medium," *J. Earth Syst. Sci.*, vol. 117, pp. 951–958, 2008.

[10] J. Ignaczak and M. Ostoja-Starzewski, *Thermoelasticity With Finite Wave Speeds*. Oxford, UK: Oxford Science Publications, 2010.

[11] Z. W. Wang, L. Y. Fu, J. Wei, W. T. Hou, J. Ba and J. M. Carcione, "On the green function of the Lord-Shulman thermoelasticity equations," *Geophys J. Int.*, vol. 220, no. 1, pp. 393–403, 2020.

[12] W. T. Hou, L. Y. Fu, J. Wei and Z. W. Wang, "Characteristic analysis of wave propagation in thermoelastic medium," *Chinese J. Geophys.*, vol. 64, no. 4, pp. 1364–1374, 2020.

[13] S. Treitel, "On the attenuation of small-amplitude plane stress waves in a thermoelastic solid," *J. Geophys. Res.*, vol. 64, no. 6, pp. 661–665, 1959.

[14] J. C. Savage, "Thermoelastic attenuation of elastic waves by cracks," *J. Geophys. Res.*, vol. 71, no. 16, pp. 3929–3938, 1966.

[15] B. H. Armstrong, "Models for thermoelastic attenuation of waves in heterogeneous solids," *Geophysics*, vol. 49, no. 7, pp. 1032–1040, 1984.

[16] M. Othman, "The uniqueness and reciprocity theorems for generalized thermo-viscoelasticity with thermal relaxation times," *Mech. Mech. Eng.*, vol. 7, no. 2, pp. 77–87, 2004.

[17] J. M. Carcione, D. Gei, J. E. Santos, L. Y. Fu and J. Ba, "Canonical analytical solutions of wave-induced thermoelastic attenuation," *Geophys. J. Int.*, vol. 221, no. 2, pp. 835–842, 2020.

[18] J. M. Carcione, F. Mainardi, S. Picotti, L. Y. Fu and J. Ba, "Thermoelasticity and P-wave simulation based on the Cole-Cole model," *J. Therm. Stress.*, vol. 43, no. 4, pp. 512–527, 2020.

[19] E. J. Wang, J. M. Carcione and J. Ba, "Wave simulation in partially saturated porothermoelastic media," *IEEE Trans. Geosci. Remote Sens.*, vol. 60, pp. 1–14, 2022.

[20] N. Noda, "Thermal stress problem in a fluid-filled porous circular cylinder," *J. Appl. Math. Mech.*, vol. 70, no. 12, pp. 543–549, 1990.

[21] D. A. Nield and A. Bejan, *Convection in Porous Media*. 3rd ed. New York: Springer, 2006.

[22] J. Wei, L. Y. Fu, Z. W. Wang, J. Ba and J. M. Carcione, "Green's function of the Lord-Shulman thermo-poroelasticity theory," *Geophys. J. Int.*, vol. 221, no. 3, pp. 1765–1776, 2020.

[23] R. Kumar, R. Vohra, and M. G. Gorla, "Variational principle and plane wave propagation in thermoelastic medium with double porosity under Lord-Shulman theory," *J. Solid Mech.*, vol. 9, no. 2, pp. 423–433, 2017.

[24] N. Q. Li, W. B. Deng, L. Y. Fu, J. M. Carcione, and T. C. Han, "Wave propagation in double-porosity thermoelastic media," *Geophysics*, vol. 87, no. 6, pp. MR265–277, 2022.

[25] J. Ba, J. M. Carcione, and J. X. Nie, "Biot-Rayleigh theory of wave propagation in double-porosity media," *J. Geophys. Res. Solid Earth*, vol. 116, no. B6, pp. 1–12, 2011.

[26] Z. W. Wang, L. Y. Fu, J. M. Carcione, W. T. Hou and J. Wei, "Analytical solution of thermoelastic attenuation in fine layering for random variations of the Grüneisen ratio," *J. Therm. Stress.*, vol. 45, no. 8, pp. 630–640, 2022.

[27] R. B. Hetnarski and J. Ignaczak, "Generalized thermoelasticity," *J. Therm. Stress.*, vol. 22, no. 4, pp. 451–476, 1999.

[28] C. Cattaneo, "Sur une Forme de l'equation de la Chaleur Eliminant le Paradoxe d'une Propagation Instantanee," *C. R. Acad. Sci.*, vol. 247, pp. 431–433, 1958.

[29] P. Vernotte, "La veritable equation de la chaleur," *C. R. Hebd. Seances Acad. Sci.*, vol. 247, pp. 2103–2015, 1958.

[30] P. Vernotte, "Les paradoxes de la theorie continue de l'equation de la chaleur," *C. R. Hebd. Seances Acad. Sci.*, vol. 246, pp. 3154–3155, 1958.
[31] D. D. Joseph and L. Preziosi, "Heat waves," *Rev. Mod. Phys.*, vol. 61, pp. 41–73, 1989.
[32] D. D. Joseph and L. Preziosi, "Addendum to the paper on heat waves," *Rev. Mod. Phys.*, vol. 62, pp. 375–391, 1990.
[33] J. Ghazanfarian, Z. Shomali and A. Abbassi, "Macro- to nanoscale heat and mass transfer: The lagging behavior," *Int. J. Thermophys.*, vol. 36, pp. 1416–1467, 2015.
[34] T. Q. Qiu and C. L. Tien, "Short-pulse laser heating on metals," *Int. J. Heat Mass Transf.*, vol. 35, no. 3, pp. 719–726, 1992.
[35] D. Y. Tzou, "A unified field approach for heat conduction from macro- to micro-scales," *ASME J. Heat Transf.*, vol. 117, no. 1, pp. 8–16, 1995.
[36] D. Y. Tzou, "The generalized lagging response in small-scale and high-rate heating," *Int. J. Heat Mass Transf.*, vol. 38, no. 17, pp. 3231–3240, 1995.
[37] D. S. Chandrasekharaiah, "Hyperbolic thermoelasticity: A review of recent literature," *APPl. Mech. Rev.*, vol. 51, no. 12, pp. 705–729, 1998.
[38] F. Xu, K. A. Seffen and T. J. Lu, "Non-Fourier analysis of skin biothermomechanics," *Int. J. Heat Mass Transf.*, vol. 51, no. 9–10, pp. 2237–2259, 2008.
[39] A. M. Abd-Alla, S. M. Abo-Dahab and A. A. Kilany, "Effect of several fields on a generalized thermoelastic medium with voids in the context of Lord-Shulman or dual-phase-lag models," *Mech. Based Des. Struct. Mach.*, vol. 50, pp. 3901–3924, 2020.
[40] M. Ragab, S. M. Abo-Dahab, A. E. Abouelregal and A. A. Kilany, "A thermoelastic piezoelectric fixed rod exposed to an axial moving heat source via a dual-phase-lag model," *Complexity*, vol. 2021, pp. 1–11, 2021.
[41] A. A. Kilany, S. M. Abo-Dahab, A. M. Abd-Alla and E. A. B. Abdel-Salam, "Non-integer order analysis of electro-magneto-thermoelastic with diffusion and voids considering Lord-Shulman and dual-phase-lag models with rotation and gravity," *Waves Random Complex Media*, pp. 1–31, 2022. DOI: 10.1080/17455030.2022.2092663.
[42] S. M. Abo-Dahab, A. M. Abd-Alla and A. A. Kilany, "Homotopy perturbation method on wave propagation in a transversely isotropic thermoelastic two-dimensional plate with gravity field," *Numer. Heat Transf. A Applic.*, vol. 82, no. 7, pp. 398–410, 2022.
[43] E. H. Saenger, N. Gold and S. A. Shapiro, "Modeling the propagation of elastic waves using a modified finite-difference grid," *Wave Motion*, vol. 31, no. 1, pp. 77–92, 2000.
[44] E. H. Saenger and S. A. Shapiro, "Effective velocities in fractured media: A numerical study using the rotated staggered finite-difference grid," *Geophysical Prospecting*, vol. 50, no. 2, pp. 183–194, 2002.
[45] W. T. Hou, L. Y. Fu, J. M. Carcione, Z. W. Wang and J. Wei, "Simulation of thermoelastic waves based on the Lord-Shulman theory," *Geophysics*, vol. 86, no. 3, pp, pp. T155–T164, 2021.
[46] D. Y. Tzou, "Nonhomogeneous lagging response in porous media: Macro to Microscale Heat Transfer," *Lagging Behav.*, vol. 3, pp. 231–253, 2014.
[47] M. N. Özişik and D. Y. Tzou, "On the wave theory in heat conduction," *J. Heat Transf.*, vol. 116, no. 3, pp. 526–535, 1994.
[48] D. Y. Tzou, "Experimental support for the lagging behavior in heat propagation," *J. Thermophys. Heat Transf.*, vol. 9, no. 4, pp. 686–693, 1995.
[49] J. M. Carcione and G. Quiroga-Goode, "Some aspects of the physics and numerical modeling of Biot compressional waves," *J. Comput. Acoust.*, vol. 3, no. 4, pp. 261–280, 1995.
[50] J. M. Carcione and G. Seriani, "Wave simulation in frozen porous media," *J. Comput. Phys.*, vol. 170, no. 2, pp. 676–695, 2001.
[51] H. E. Elsayed-Ali, "Femtosecond thermoreflectivity and thermotrans-missivity of polycrystalline and single-crystalline gold films," *Physical Rev. B*, vol. 43, pp. 4488–4491, 1991.
[52] R. H. M. Groeneveld, R. Sprik and A. Lagendijk, "Ultrafast relaxation of electrons probed by surface plasmons at a thin silver film," *Phys. Rev. Lett.*, vol. 64, no. 7, pp. 368–370, 1990.
[53] A. G. Agwu Nnanna, A. Haji-Sheikh and K. T. Harris, "Experimental study of local thermal non-equilibrium phenomena during phase change in porous media," *Int. J. Heat Mass Transf.*, vol. 47, pp. 4365–4375, 2004.
[54] A. G. Agwu Nnanna, A. Haji-Sheikh and K. T. Harris, "An experimental study of non-Fourier thermal response in porous media," *J. Porous Media*, vol. 8, pp. 31–44, 2005.
[55] E. Kjartansson, "Attenuation of seismic waves in rocks and applications in energy exploration," Ph.D. thesis, Stanford, CA: Stanford University, 1979.